Microsc. Microanal. 17, 582–586, 2011
doi:10.1017/S1431927611000286

Microscopy AND Microanalysis

© MICROSCOPY SOCIETY OF AMERICA 2011

Carbon Diffusion from Methane into Walls of Carbon Nanotube through Structurally and Compositionally Modified Iron Catalyst

Michael J. Behr, K. Andre Mkhoyan,* and Eray S. Aydil*

Department of Chemical Engineering and Materials Science, University of Minnesota, Minneapolis, MN 55455, USA

Abstract: To understand diffusion processes occurring inside Fe catalysts during multiwall carbon nanotube (MWCNT) growth, catalysts were studied using atomic-resolution scanning transmission electron microscopy combined with electron energy-loss spectroscopy. Nanotube walls emanate from structurally modified and chemically complex catalysts that consist of cementite and a 5 nm amorphous FeO_x cap separated by a 2–3 nm thick carbon-rich region that also contains Fe and O (a-C:Fe_xO_y). Nonuniform distribution of carbon atoms throughout the catalyst base reveals that carbon molecules from the gas phase decompose near the catalyst multisection junction, where the MWCNT walls terminate. Formation of the a-C:Fe_xO_y region provides the essential carbon source for MWCNT growth. Two different carbon diffusion mechanisms are responsible for the growth of the inner and outer walls of each MWCNT.

Key words: carbon nanotube, catalyst, iron, cementite, diffusion, STEM, EELS

Introduction

Wide-ranging applications of carbon nanotubes (CNTs) that utilize their unique electronic and optical properties rely on precise control of the CNT structure. Despite many promising results reported in the last two decades, a high level of structural control has not yet been achieved (Tans et al., 1998; Baughman et al., 2002; Dresselhaus et al., 2004; Barone et al., 2005). Plasma-enhanced chemical vapor deposition (PECVD), which uses hydrocarbon gas mixtures with iron, cobalt, or nickel catalyst nanoparticles, enables large-scale growth with controlled spatial placement of CNTs on a substrate (Ren et al., 1998; Melechko et al., 2005; Meyyappan, 2009). During nanotube growth, specifically when multiwall carbon nanotubes (MWCNTs) are considered, hydrocarbon molecules and radicals from the gas phase decompose on the catalyst surface and provide the source of carbon atoms that diffuse and add to the base of the growing MWCNT walls. However, the understanding of the exact chemical and diffusion processes occurring inside the metal catalyst that lead to the formation of nanotube walls still needs clarification.

When Fe-based catalysts were used, MWCNTs have been reported to grow not only from metallic Fe in body- and face-centered cubic phases, but also from the cementite (Fe_3C) phase that forms *in situ* when the Fe catalyst is exposed to carbon during growth (Blank et al., 2002; Yoshida et al., 2008; Sharma et al., 2009). It was speculated that Fe_3C plays an intermediate role and that the surface of the Fe_3C catalyst decomposes into Fe metal and graphite producing the CNT walls (Schaper et al., 2004; Kim & Sigmund, 2005; Golberg et al., 2006; Rodríguez-Manzo et al., 2007). *Ab initio* calculations and molecular dynamics simulations have predicted low energy barriers for carbon diffusion on the surface of Fe catalyst particles (Hofmann et al., 2005; Raty et al., 2005). Although some experimental studies support the possibility that carbon diffusion occurs on the catalyst surface (Helveg et al., 2004; Hofmann et al., 2005; Begtrup et al., 2009), others indicate that diffusion might occur through the bulk of iron-based catalysts (Rodríguez-Manzo et al., 2007; Yoshida et al., 2008; Wirth et al., 2009).

In this article, we present a detailed atomic-level examination of the structural and compositional changes that take place in iron catalysts during CNT growth using quantitative high-resolution scanning transmission electron microscopy (STEM) combined with electron energy-loss spectroscopy (EELS). STEM with EELS provides a unique combination of atomic-resolution imaging with parallel spectroscopy (Batson, 1993*a*) and, therefore, it is often the method of choice for measuring atomic-scale compositional changes in nanomaterials (Mkhoyan et al., 2004; Enache et al., 2006; Bosman et al., 2007; Carlson et al., 2007). The results presented herein clarify the discussion of the diffusion mechanisms for carbon atoms from methane molecules into the walls of MWCNTs during nanotube growth. Structural and compositional changes taking place inside initially Fe catalyst particles to accommodate such diffusion are also presented.

Materials and Methods

MWCNTs studied here were grown using a radio-frequency (at 13.56 MHz) inductively-coupled plasma from initially pure Fe catalysts through PECVD. The Fe catalyst was deposited as a 10 nm thick film on native-oxide-coated silicon substrates using electron-beam evaporation. Before nanotube growth, the catalyst film was heated to 700°C and ex-

Received October 26, 2010; accepted February 28, 2011
**Corresponding authors*. E-mail: mkhoyan@umn.edu, aydil@umn.edu

posed for 15 min to an H_2:Ar = 50:5 sccm plasma maintained at 200 W power and 150 mTorr pressure, a treatment that converts the continuous Fe film into nanometer-size metal islands. MWCNTs were grown at 800°C and 10 Torr for 30 min using a plasma maintained at 200 W power in a CH_4:H_2:Ar = 5:5:68 sccm gas mixture. Under these growth conditions, the catalyst particles produce systematic high-quality MWCNTs with an average outer diameter of 29 ± 5 nm. The details of the growth conditions and their effects on catalyst particles and MWCNT structure have been reported earlier (Behr et al., 2010*a*, 2010*b*).

The MWCNTs were examined in a FEI (Hillsboro, OR, USA) Tecnai F-30 (S)TEM operated at 300 keV that produces a focused ~1.5 Å diameter electron probe when operated as a STEM. Nanotubes were removed from the Si/SiO_2 substrate by sonication in ethanol for 30 s and then transferred to a copper TEM grid coated with a holey carbon support film by drop casting from this solution (Behr et al., 2010*a*, 2010*b*, 2010*c*). The (S)TEM is equipped with a Schottky field-emission electron gun, low-angle and high-angle annular dark field (LAADF and HAADF) detectors and a Gatan Enfina-1000 EELS. The energy resolution of the spectrometer, measured using the full-width at half-maximum of the zero-loss peak, was ~0.5 eV. The chemical composition of the catalysts was measured by recording ADF images and core-level EELS spectra of the components: Fe $L_{2,3}$-edge, C and O K-edges with 8, 4, and 6 s acquisition times, respectively. Operation of the STEM was optimized in such a way to minimize electron-beam-induced damage. STEM-EELS results presented here have negligible electron beam damage. For these operational conditions heating of the specimen is also negligible (<1°C). EELS measurements were conducted from the portion of the samples hanging over a hole in the carbon support to avoid additional carbon signal from the support. Tests on contamination were also performed, and no detectable contamination was observed.

Results

Two examples of typical catalysts observed inside the base of the MWCNTs are shown in Figure 1a–c. The MWCNTs grown from these catalysts are vertically aligned and perpendicular to the substrate, whereby the catalysts remain attached to the substrate, as shown schematically in Figure 1d. The catalysts exhibited an elongated tear-drop shape with a smooth taper on faces oriented approximately parallel to the MWCNT axis. Systematic characterization of the MWCNTs and the catalyst particles obtained using our PECVD recipe, including MWCNTs used in this study, was reported earlier (Behr et al., 2010*a*).

Figure 1c shows a composition-sensitive HAADF image of the catalyst base. Three distinct regions can be identified. The brightest region at the top that constitutes the largest portion of the catalyst is single crystal cementite (Fe_3C). The Fe_3C was identified after establishing its crystal structure by completing the full diffraction map and by confirming its composition using the Fe $L_{2,3}$- and C K-edges in EELS (Behr et al., 2010*b*). The brighter ~5 nm thick region at the base, appearing like a cap, was studied with EELS, energy dispersive X-ray (EDX) spectroscopy, and diffraction. This study (Fig. 1d,f) revealed that this layer is predominantly amorphous FeO_x (a-FeO_x) with a small amount of carbon. This oxide cap is formed from catalyst interaction with the native oxide on the silicon substrate. Interestingly, the MWCNT walls, barely visible in HAADF images, do not extend all the way to the base but instead terminate at the a-FeO_x, ~12 nm above the base of the a-FeO_x cap. The EELS and EDX measurements also indicate that this PECVD-based MWCNT growth produces catalyst nanoparticles with no detectable amount of Si present inside, unlike the modified Fe catalyst nanoparticles prepared by thermal CVD (Yao et al., 2004*a*, 2004*b*).

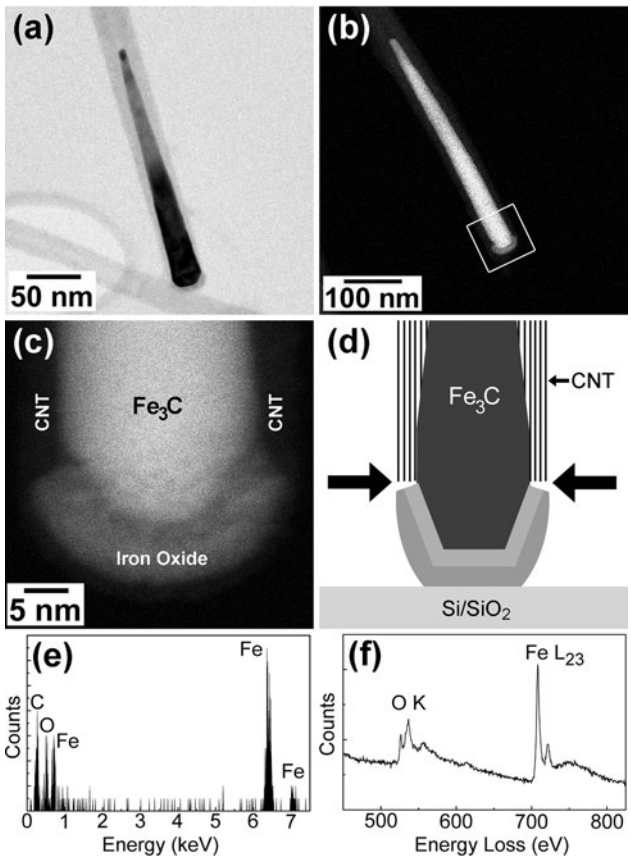

Figure 1. (**a**) Phase-contrast TEM image of a catalyst located inside the base of a MWCNT. (**b**) HAADF STEM image of another catalyst inside the base of a MWCNT. (**c**) Magnified HAADF STEM image of the catalyst base showing three distinct sections. (**d**) Schematic of the catalyst base region with arrows indicating the locations where C from the gas phase enters into the catalyst. (**e**) EDX and (**f**) EELS spectra from the a-FeO_x shell.

Examination of many catalysts revealed the systematic presence of a 2–3 nm thick region between the a-FeO_x and the Fe_3C that appears darker than the a-FeO_x in composition-sensitive HAADF images. The darker contrast indicates that the average atomic number in this region is lower than in a-FeO_x. Examination of the EELS spectra of C and O K-

and Fe $L_{2,3}$-edges collected from this region and comparison with spectra from the Fe_3C, a-FeO_x cap and MWCNT walls, shown in Figure 2a,b, revealed that this interfacial region is amorphous, carbon-rich, and contains Fe and O. Hereafter, we refer to this layer as a-C:Fe_xO_y. In contrast to C K-edge spectra measured from the CNT and Fe_3C, the fine structure of the C K-edge obtained from this layer lacks distinct features. Specifically, neither the π^* peak at 285.5 eV nor σ^* peak at 292.5 eV are evident. This lack of fine structure in the core-loss edge is indicative of the C K-edge EELS spectrum obtained from carbon in an amorphous state (Batson, 1993*b*; Egerton, 1996; Huang, 1999).

To map the carbon distribution inside the catalyst particle, atomic-scale EELS measurements of the C K-edge were acquired throughout the base of the catalyst. The spectra were measured every 0.6 nm along the specific lines indicated in Figure 2c. The integrated intensity of the C K-edge was calculated for each probe position, and the results are presented in Figure 2d. These intensities were calculated by integrating the C K-edge signal over a 30 eV wide window aligned with the onset of the edge, after subtracting the background (backgrounds were subtracted using the conventional $f(E) = A \cdot E^{-r}$ fitting function). Corrections for changes in specimen thickness along each line were also made based on the geometry of the catalyst. The shape and features of the C K-edge EELS spectrum, shown in Figure 2a, remained the same throughout each line examined, and thus the measured integrated intensity can be treated as a direct measure of the relative carbon concentration.

The carbon distribution map shows significant variations in carbon concentration at the bottom part of the mostly Fe_3C catalyst and, in particular, in the thin a-C:Fe_xO_y region. The highest measured carbon concentration was near the triple junction formed by Fe_3C, a-FeO_x, and the MWCNT walls. Carbon concentration was found to decrease significantly as the electron probe moved along any line away from this triple junction. Comparison between adjacent line scans (see Fig. 2d) reveals that the carbon concentration increases with radial position inward from the a-FeO_x cap toward the Fe_3C crystal. This increase in carbon concentration is not gradual but exhibits a jump at ~3 nm outside the faceted Fe_3C, which coincides with the start of the carbon-rich a-C:Fe_xO_y region.

As the high-resolution TEM and STEM images show, the outer walls of the MWCNT terminate at the triple junction and the inner walls at the tapered surfaces of the Fe_3C crystal. These indicate that the MWCNT growth mechanism is robust and not specific to a particular interface or surface of the catalyst. The images also show that the outer layers of the MWCNTs are not terminated at the iron oxide cap and a gap may be present between the cap and the walls, which terminates at the triple junction (see Fig. 1d). A graphene edge and a carbon source are all that is required to sustain the growth. However, carbon has to reach the walls emanating from the base of the catalyst as well as those emanating from the tapered side walls of the catalyst for the MWCNT to grow.

The gradients in carbon concentration through the catalyst base and the presence of a carbon-rich a-C:Fe_xO_y region between the Fe_3C and a-FeO_x cap provide important clues as to the chemical and diffusion processes responsible for MWCNT growth. Substantially higher carbon concentrations were measured near the triple junction. Thus, carbon or carbon-containing molecular fragments (e.g., CH_x) must diffuse between the FeO_x cap and the MWCNT walls. Here, carbon atoms directly add to the existing graphene ring edges to sustain the growth. This is consistent with our observations of a concentration decrease as one moves away from the triple junction and with the presence a carbon-rich a-C:Fe_xO_y region (see Fig. 2c,d).

The presence of an ~10 eV energy barrier for carbon atoms to penetrate through a hexagonal hole in graphene (Xu et al., 1993; Rodríguez-Manzo et al., 2007) and our observations that MWCNTs do not grow when catalyst particles are completely covered in graphene shells eliminates the possibility for carbon diffusion through the MWCNT walls. Since carbon concentration measured in the FeO_x cap is about 5× lower than in the rest of the catalyst (see Fig. 2d), the diffusion through the substrate is not realistic either. This leaves diffusion through the triple junction as the main possible path for carbon incorporation into the outer walls of the growing MWCNT.

A remaining issue is how carbon atoms reach and add to the inner MWCNT walls attached to the tapered surfaces of the Fe_3C crystal. The nanotube inner walls were observed to form at two locations on the Fe_3C catalyst; cylindrical walls grew from the long tapered catalyst face, and the graphene cup structures formed at the rounded catalyst end, opposite from the catalyst base as indicated in Figure 3a. Diffusion through the MWCNT walls is eliminated as a possibility based on high activation energy barriers for diffusion, as discussed previously. All MWCNT walls grow at the same rate, which indicates that the addition of the carbon to the graphene edges must limit the growth. This also indicates that the diffusion processes must be fast. Thus, we surmise that the carbon rapidly diffuses from the triple junction along the Fe_3C/CNT interface. The high concentration of carbon in the triple junction, particularly in the a-C:Fe_xO_y region, suggests that this layer acts as the carbon source.

It was also speculated that inner walls of MWCNTs can grow from Fe_3C by a process similar to "metal dusting" (Grabke, 2003), whereby the surface of the Fe_3C crystal decomposes into Fe metal and graphene walls (Kim & Sigmund, 2005; Golberg et al., 2006). Thus, if this is the case, a thin layer of metallic Fe is expected to exist at the Fe_3C/CNT interface. A high-resolution ADF image of this Fe_3C/CNT interface is shown in Figure 3b. We tested "metal dusting" as a possible growth mechanism by using STEM-EELS to measure the Fe $L_{2,3}$-edge at this interface and compare it to the Fe $L_{2,3}$-edge measured in the Fe_3C crystal (see Fig. 3c). The Fe $L_{2,3}$-edge, which is composed of two "white lines" resulting from electronic transitions from initial $2p^{1/2}$ and $2p^{3/2}$ core states to the empty states above the

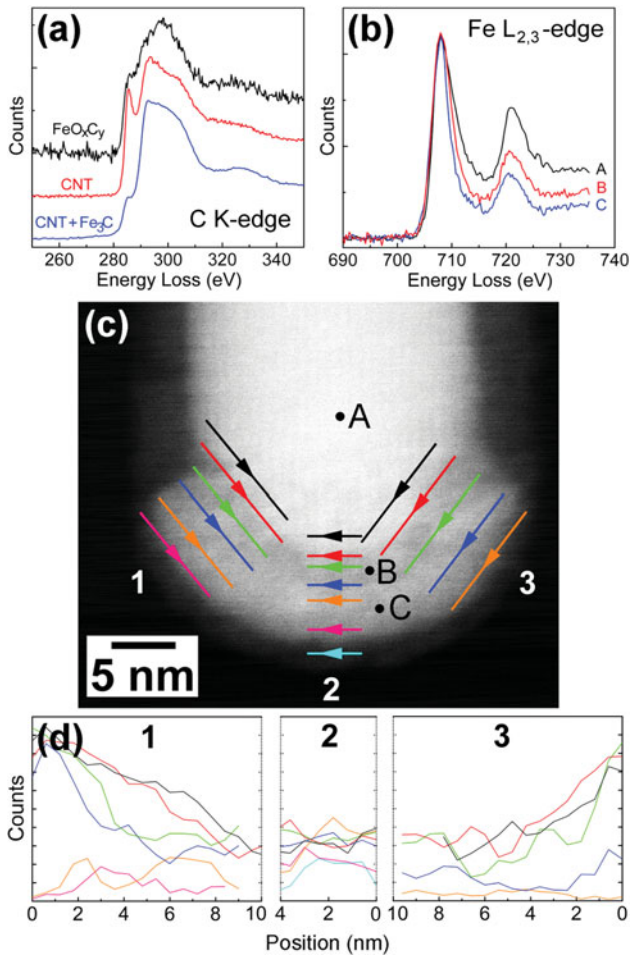

Figure 2. (**a**) Normalized EELS spectra of the C K-edge measured from the CNT, Fe_3C covered with the CNT and from the interfacial region, and (**b**) the Fe $L_{2,3}$-edge measured from the positions A, B, and C with L_2/L_3 peak intensity ratios of 0.65 ± 0.06, 0.44 ± 0.04, and 0.35 ± 0.03, respectively. (**c**) High-resolution LAADF STEM image of the catalyst base with lines indicating locations and directions of the mapping probe. (**d**) Relative carbon concentration, as calculated from measured C K-edges. Plot colors correspond to the colored lines in panel **c**.

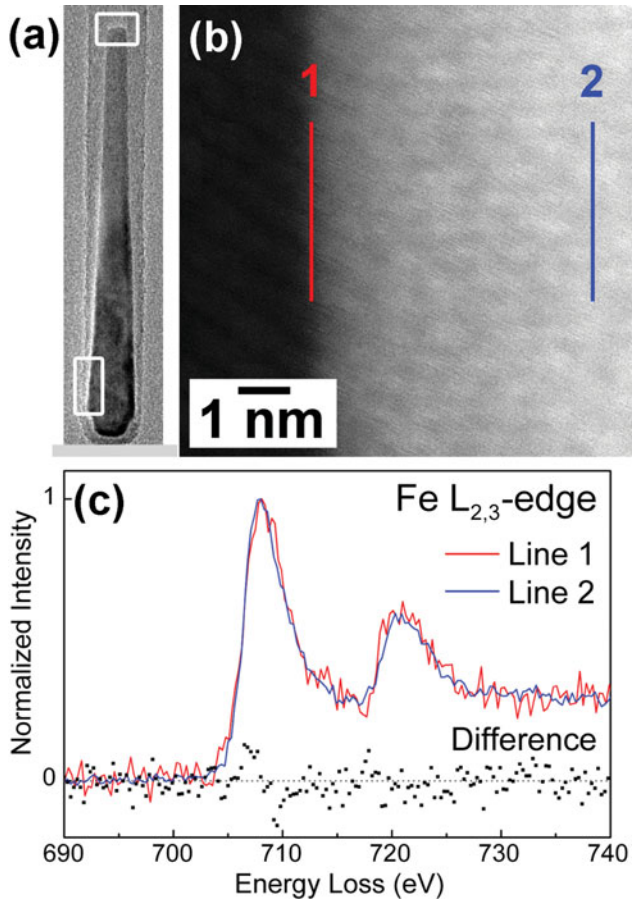

Figure 3. (**a**) Phase-contrast TEM image of the catalyst inside the base of a MWCNT. Rectangles indicate regions of CNT wall growth, where the Fe $L_{2,3}$-edge was measured. (**b**) LAADF image of the Fe_3C/CNT interface. (**c**) Normalized average Fe $L_{2,3}$-edges measured every 0.3 nm along the length of two lines, shown in panel **b** and the difference.

Fermi level, is expected to have an overall downward shift of ~0.7 eV at onset and ~1.5 eV decrease in spacing between the two peaks for Fe metal as compared to Fe_3C (Jin et al., 2006). The difference between the two spectra is shown also in Figure 3c. The two spectra are practically identical, and therefore no metallic Fe layer exists between Fe_3C and the CNT walls. Similar results were also obtained from other regions of the catalyst, near the rounded tip as indicated in Figure 3a.

Conclusions

In conclusion, we observe that systematic high-quality MWCNTs grow from complex catalyst nanoparticles that consist of two main components: cementite and an a-FeO_x cap separated by a 2–3 nm carbon-rich a-C:Fe_xO_y region, and a strong gradient in carbon concentration exists from the surface to the center at the catalyst base. These observations indicate that gas-phase carbonaceous species decompose at the triple junction of Fe_3C, a-FeO_x, and MWCNT walls and that these decomposed carbon atoms, now in the a-C:Fe_xO_y region, directly incorporate into the outer nanotube walls or diffuse upward along the Fe_3C/CNT interface to produce MWCNT inner walls. Some slow diffusion through the bulk of Fe_3C can also be expected. Atomic-scale EELS measurements show that the chemical state of Fe_3C does not change at the Fe_3C/CNT interface and therefore eliminates "metal dusting" as a possible carbon incorporation pathway.

Acknowledgments

The authors thank Dr. O. Ugurlu for technical support. This work was partially supported by National Science Foundation (NSF) grant CBET-0613629 and utilized the University of Minnesota Characterization Facility, which receives partial support from the NSF-NNIN program and capital equipment funding from the NSF-MRSEC program DMR-0819885.

References

Barone, P.W., Baik, S., Heller, D.A. & Strano, M.S. (2005). Near-infrared optical sensors based on single-walled carbon nanotubes. *Nat Mater* **4**, 86–92.

Batson, P.E. (1993*a*). Simultaneous STEM imaging and electron energy-loss spectroscopy with atomic-column sensitivity. *Nature* **366**, 727–728.

Batson, P.E. (1993*b*). Carbon 1s near-edge-absorption fine structure in graphite. *Phys Rev B* **48**, 2608–2610.

Baughman, R.H., Zakhidov, A.A. & de Heer, W.A. (2002). Carbon nanotubes—The route toward applications. *Science* **297**, 787–792.

Begtrup, G.E., Gannett, W., Meyer, J.C., Yuzvinsky, T.D., Ertekin, E., Grossman, J.C. & Zettl, A. (2009). Facets of nanotube synthesis: High-resolution transmission electron microscopy study and density functional theory calculations. *Phys Rev B* **79**, 205409.

Behr, M.J., Gaulding, E.A., Mkhoyan, K.A. & Aydil, E.S. (2010*a*). Effects of hydrogen on catalyst nanoparticles in carbon nanotube growth. *J Appl Phys* **108**, 053303.

Behr, M.J., Mkhoyan, K.A. & Aydil, E.S. (2010*b*). Orientation and morphological evolution of catalyst nanoparticles during carbon nanotube growth. *ACS Nano* **4**, 5087–5094.

Behr, M.J., Mkhoyan, K.A. & Aydil, E.S. (2010*c*). Catalyst rotation, twisting, and bending during multiwall carbon nanotube growth. *Carbon* **48**, 3840–3845.

Blank, V.D., Kulnitskiy, B.A., Batov, D.V., Bangert, U., Gutiérrez-Sosa, A. & Harvey, A.J. (2002). Electron microscopy and electron energy loss spectroscopy studies of carbon fiber formation at Fe catalysts. *J Appl Phys* **91**, 1657–1660.

Bosman, M., Keast, V.J., García-Muñoz, J.L., D'Alfonso, A.J., Findlay, S.D. & Allen, L.J. (2007). Two-dimensional mapping of chemical information at atomic resolution. *Phys Rev Lett* **99**, 086102.

Carlson, L.J., Maccagnano, S.E., Zheng, M., Silcox, J. & Krauss, T.D. (2007). Fluorescence efficiency of individual carbon nanotubes. *Nano Lett* **7**, 3698–3703.

Dresselhaus, M.S., Dresselhaus, G., Charlier, J.C. & Hernandez, E. (2004). Electronic, thermal and mechanical properties of carbon nanotubes. *Phil Trans R Soc Lond* **362**, 2065–2098.

Egerton, R. (1996). *Electron Energy Loss Spectroscopy in the Electron Microscope*. New York: Plenum.

Enache, D.I., Edwards, J.K., Landon, P., Solsona-Espriu, B., Carley, A.F., Herzing, A.A., Watanabe, M., Kiely, C.J., Knight, D.W. & Hutchings, G.J. (2006). Solvent-free oxidation of primary alcohols to aldehydes using Au-Pd/TiO_2 catalysts. *Science* **311**, 362–365

Golberg, D., Mitome, M., Muller, C., Tang, C.C., Leonhardt, A. & Bando, Y. (2006). Atomic structures of iron-based single-crystalline nanowires crystallized inside multi-walled carbon nanotubes as revealed by analytical electron microscopy. *Acta Mater* **54**, 2567–2576.

Grabke, H.J. (2003). Metal dusting. *Mater Corros* **54**, 736–740.

Helveg, S., López-Cartes, C., Sehested, J., Hansen, P.L., Clausen, B.S., Rostrup-Nielsen, J.R., Abild-Pedersen, F. & Nørskov, J.K. (2004). Atomic-scale imaging of carbon nanofibre growth. *Nature* **427**, 426–429.

Hofmann, S., Csanyi, G., Ferrari, A.C., Payne, M.C. & Robertson, J. (2005). Surface diffusion: The low activation energy path for nanotube growth. *Phys Rev Lett* **95**, 036101.

Huang, J.Y. (1999). HRTEM and EELS studies of defects structure and amorphous-like graphite induced by ball milling. *Acta Mater* **47**, 1801–1808.

Jin, Y.M., Xu, H.F. & Datye, A.K. (2006). Electron energy loss spectroscopy (EELS) of iron Fischer-Tropsch catalysts. *Microsc Microanal* **12**, 124–134.

Kim, H. & Sigmund, W. (2005). Iron particles in carbon nanotubes. *Carbon* **43**, 1743–1748.

Melechko, A.V., Merkulov, V.I., McKnight, T.E., Guillorn, M.A., Klein, K.L., Lowndes, D.H. & Simpson, M.L. (2005). Vertically aligned carbon nanofibers and related structures: Controlled synthesis and directed assembly. *J Appl Phys* **97**, 041301.

Meyyappan, M. (2009). A review of plasma enhanced chemical vapour deposition of carbon nanotubes. *J Phys D Appl Phys* **42**, 213001.

Mkhoyan, K.A., Kirkland, E.J., Silcox, J. & Alldredge, E.S. (2004). Atomic-level characterization of GaN/AlN quantum wells. *J Appl Phys* **96**, 738–741.

Raty, J.Y., Gygi, F. & Galli, G. (2005). Growth of carbon nanotubes on metal nanoparticles: A microscopic mechanism from *ab initio* molecular dynamics simulations. *Phys Rev Lett* **95**, 096103.

Ren, Z.F., Huang, Z.P., Xu, J.W., Wang, J.H., Bush, P., Siegal, M.P. & Provencio, P.N. (1998). Synthesis of large arrays of well-aligned carbon nanotubes on glass. *Science* **282**, 1105–1107.

Rodríguez-Manzo, J.A., Terrones, M., Terrones, H., Kroto, H.W., Sun, L. & Banhart, F. (2007). *In situ* nucleation of carbon nanotubes by the injection of carbon atoms into metal particles. *Nat Nanotechnol* **2**, 307–311.

Schaper, A.K., Hou, H.Q., Greiner, A. & Phillipp, F. (2004). The role of iron carbide in multiwalled carbon nanotube growth. *J Catal* **222**, 250–254.

Sharma, R., Moore, E., Rez, P. & Treacy, M.M.J. (2009). Site-specific fabrication of Fe particles for carbon nanotube growth. *Nano Lett* **9**, 689–694.

Tans, S.J., Verschueren, A.R.M. & Dekker, C. (1998). Room-temperature transistor based on a single carbon nanotube. *Nature* **393**, 49–52.

Wirth, C.T., Zhang, C., Zhong, G.F., Hofmann, S. & Robertson, J. (2009). Diffusion- and reaction-limited growth of carbon nanotube forests. *ACS Nano* **3**, 3560–3566.

Xu, C.H., Fu, C.L. & Pedraza, D.F. (1993). Simulations of point-defect properties in graphite by a tight-binding-force model. *Phys Rev B* **48**, 13273–13279.

Yao, Y., Falk, L.K.L., Morjan, R.E., Nerushev, O.A. & Campbell, E.E.B. (2004*a*). Synthesis of carbon nanotube films by thermal CVD in the presence of supported catalyst particles. Part I: The silicon substrate/nanotube film interface. *J Mater Sci Mater Electron* **15**, 533–543.

Yao, Y., Falk, L.K.L., Morjan, R.E., Nerushev, O.A. & Campbell, E.E.B. (2004*b*). Synthesis of carbon nanotube films by thermal CVD in the presence of supported catalyst particles. Part II: The silicon substrate/nanotube film interface. *J Mater Sci Mater Electron* **15**, 583–594.

Yoshida, H., Takeda, S., Uchiyama, T., Kohno, H. & Homma, Y. (2008). Atomic-scale in-situ observation of carbon nanotube growth from solid state iron carbide nanoparticles. *Nano Lett* **8**, 2082–2086.